Increasing the Potential of the Auristatin Cancer-Drug Family by Shifting the Conformational Equilibrium

Sokka, Iris Katariina

2019-08

Sokka , I K , Ekholm , F S & Johansson , M P 2019 , ' Increasing the Potential of the Auristatin Cancer-Drug Family by Shifting the Conformational Equilibrium ' , Molecular Pharmaceutics , vol. 16 , no. 8 , pp. 3600-3608 . https://doi.org/10.1021/acs.molpharmaceut.9b00437

http://hdl.handle.net/10138/304573
https://doi.org/10.1021/acs.molpharmaceut.9b00437

molecular pharmaceutics

Article

Cite This: Mol. Pharmaceutics 2019, 16, 3600−3608

pubs.acs.org/molecularpharmaceutics

Increasing the Potential of the Auristatin Cancer-Drug Family by Shifting the Conformational Equilibrium

Iris K. Sokka,[†] Filip S. Ekholm,[†] and Mikael P. Johansson*[,†,‡]

[†]Department of Chemistry, University of Helsinki, P.O. Box 55, FI-00014 Helsinki, Finland

[‡]Helsinki Institute of Sustainability Science, HELSUS, FI-00014 Helsinki, Finland

Supporting Information

ABSTRACT: Monomethyl auristatin E and monomethyl auristatin F are widely used cytotoxic agents in antibody−drug conjugates (ADCs), a group of promising cancer drugs. The ADCs specifically target cancer cells, releasing the auristatins inside, which results in the prevention of mitosis. The auristatins suffer from a potentially serious flaw, however. In solution, the molecules exist in an equal mixture of two conformers, cis and trans. Only the trans-isomer is biologically active and the isomerization process, i.e., the conversion of cis to trans is slow. This significantly diminishes the efficiency of the drugs and their corresponding ADCs, and perhaps more importantly, raises concerns over drug safety. The potency of the auristatins would be enhanced by decreasing the amount of the biologically inactive isomer, either by stabilizing the trans-isomer or destabilizing the cis-isomer. Here, we follow the computer-aided design strategy of shifting the conformational equilibrium and employ high-level quantum chemical modeling to identify promising candidates for improved auristatins. Coupled cluster calculations predict that a simple halogenation in the norephedrine/phenylalanine residues shifts the isomer equilibrium almost completely toward the active trans-conformation, due to enhanced intramolecular interactions specific to the active isomer.

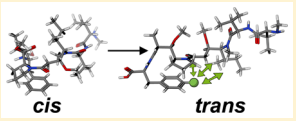

KEYWORDS: *cytotoxicity, molecular modeling, computer-aided drug design, intramolecular interactions, quantum chemistry, drug development*

INTRODUCTION

Monomethyl auristatin E (MMAE) and monomethyl auristatin F (MMAF) are cell cytotoxic agents that bind to microtubules and prevent cell proliferation by inhibiting mitosis.[1−5] They are used as warheads in a number of state-of-the-art antibody−drug conjugates (ADCs).[6−10] The efficiency of ADCs is based on the highly selective targeting capabilities of the antibodies. The antibody binds to certain proteins that the target, the diseased cell, expresses more than the regular cells of the body.[6,11] Upon reaching their destination, i.e., the cancer cells expressing the correct antigen, they are internalized by endocytosis.[6,12] Once inside the cell, the cytotoxic warhead molecule, e.g., the auristatin, is released from the antibody, causing cell death. Ideally, an ADC destroys the target cell without causing harm to other cells, thus working like the "magic bullets" envisioned by Paul Ehrlich at the beginning of the 20th century.[13−22]

Like other cancer drugs that work by preventing cell division, the side-effects caused by the auristatins arise from their effects on the normal, quickly dividing cell-types of the body. In fact, the auristatins are too toxic to be used as such and are only used as part of ADCs in current treatments. Common side-effects of ADCs with the auristatin include neutropenia, neuropathy, thrombocytopenia, and ocular toxicities.[23−25]

The schematic structures of MMAE and MMAF are shown in Figure 1. Both are composed of five amino acids. MMAE consists of norephedrine, dolaproine, dolaisoleuine, valine, and monomethyl valine. In MMAF, the C-terminal norephedrine is

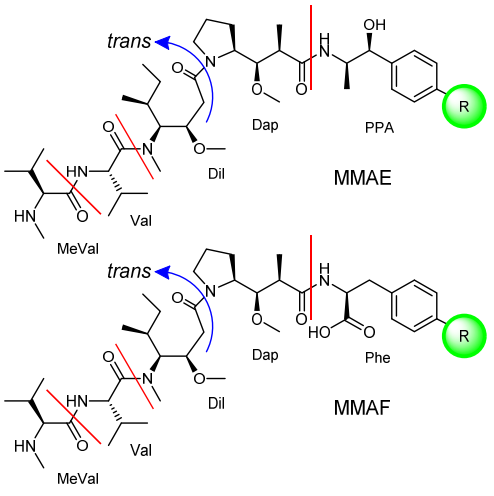

Figure 1. Molecular structures of MMAE (top) and MMAF (bottom) in their cis conformations, and their constituent amino acids: monomethyl valine (MeVal), valine (Val), dolaisoleuine (Dil), dolaproine (Dap), and norephedrine (PPA)/phenylalanine (Phe). The site of modification considered here, R, is marked in green. The blue arrow shows the peptide bond rotation leading to the trans-isomer.

Received: April 24, 2019
Revised: June 6, 2019
Accepted: June 14, 2019
Published: June 14, 2019

DOI: 10.1021/acs.molpharmaceut.9b00437
Mol. Pharmaceutics 2019, 16, 3600−3608

replaced by phenylalanine. Recently, it was found that both MMAE and MMAF exist as two different conformational isomers, denoted cis and trans with respect to the amide bond between dolaproine and dolaisoleuine.[22] In solution, the two conformers have roughly equal proportions, but only one, the trans-form, is biologically active.[26]

Now, to abate side-effects, drug dosage should naturally be kept at a minimum, while still reaching the desired potency. In light of this, the fact that half of the auristatins delivered by ADCs are ineffective is disquieting. Although it is true that the inactive cis-conformer does isomerize to the active trans-form by rotation around an amide bond, this process takes several hours as the rotational energy barrier around the amide bond is high (ca. 100 kJ/mol).[22] Therefore, the auristatins may already have escaped the confinements of the targeted cancer cells when they are transformed into active components, thus potentially causing damage to healthy cells. This indication is supported by recent studies on the hydrophobic nature of auristatins.[27]

A good starting point for improving the properties of ADCs would be to optimize the cytotoxic warheads currently in use. In fact, modification of auristatins has been an active field of study since the original modifications to dolastatin 10 itself,[1,28,29] with various aspects of the drug molecules tuned.[27,30−37] Modifying the auristatins with the explicit goal of decreasing the potential for side-effects caused by the presence of the dormant, biologically inactive cis-conformer is a hitherto overlooked strategy, however. There are a couple of alternatives for achieving this. If the barrier for conversion between cis and trans could be lowered so much that the interconversion would be significantly faster, the drug molecules would become active before leaving the diseased cell. To decrease the time needed for conversion from hours to, say, seconds, the rotational barrier would have to be lowered by roughly 25 kJ/mol. This would, however, be difficult for the rather rigid peptide bond. Alternatively, the rotational barrier could be further increased, practically locking the conformation to either isomer. This might be possible with suitable modifications to the structure, although rather bulky ligands would probably be needed, affecting also tubulin binding.

An ideal modification would instead of modifying the barrier, shift the equilibrium from a 60:40 cis/trans distribution toward the trans-conformer; then, the drug dosage as such could be halved, and the problem of conversion between cis and trans would be diminished. Here, using high-level quantum mechanical modeling at the coupled-cluster CCSD(T) level, we investigate what kind of structural modification could afford such a conformational equilibrium shift in the auristatins, while at the same time maintaining a rather intact binding affinity to tubulin.

In general, accurately modeling ligand binding to large biomolecules is a daunting task. In their comprehensive review on the use of quantum chemical methods for estimating binding affinities, Ryde and Söderhjelm[38] highlight the main problem of quantum mechanical studies: the limitations on conformational sampling imposed by the computational cost of an otherwise accurate methodology. Although steps toward solving the sampling problem are continuously taken, there is still some way to go.[39−46] From this perspective, the auristatins are a rather agreeable object of study. Previously, by combining NMR spectroscopy and quantum chemical modeling, we showed that in solution, MMAE and MMAF exist as a mixture of only two conformations; other structures are not present in concentrations detectable by NMR.[22] The same holds true for other auristatin derivatives synthesized in the past.[34] Thus, we here have a case where high-accuracy modeling is viable also in molecular pharmaceutics, due to the limited conformational space of the drug molecules.

Below, we show that an almost complete shift toward the trans-isomer can be achieved by a minimal change to the molecular structure: halogenation of the norephedrine and phenylalanine residues in MMAE and MMAF, respectively.

METHODS

The geometries were optimized at density functional theory (DFT) level,[47] using the hybrid Tao−Perdew−Staroverov−Scuseria functional corrected for dispersion interactions, TPSSh-D3(BJ),[48−51] with the def2-TZVPP (for isomer energy differences) and def2-SVP (for vibrational frequencies and the tubulin−MMAE complex) basis sets.[52] Solvation effects were accounted for with the COSMO model.[53] Final electronic energies were computed at the domain-based local pair natural orbital DLPNO-CCSD(T) coupled cluster level of theory,[54−56] extrapolating toward the complete basis set limit using the two-point formula by Halkier et al.[57] in connection with the def2-TZVPPD and def2-QZVPPD triple- and quadruple-ζ basis set augmented with diffuse functions.[52,58] Enthalpies and free energies were estimated from the harmonic vibrational frequencies, with possible low-frequency modes below 50 cm^{-1} set to 50 cm^{-1}, using gas-phase structures and frequencies. For the tubulin models, the contributions from the fixed atoms were discarded. We note the good agreement between simulation and experiment for the original MMAE and MMAF (see Table 3), corroborating the suitability of the present level of theory, as reported also in previous studies.[59−61] Intramolecular, noncovalent interaction (NCI) energies were computed using F/I-SAPT0,[62−64] in connection with the Pauling point[65] providing the jun-cc-pVDZ basis set,[66] without implicit solvent. For the symmetry-adapted perturbation theory (SAPT) analysis, the fragments were divided after the peptide bond (counting from the C-terminus) to perform the cut at a single σ-bond, instead of cutting the actual OC−NH bond. The tubulin−MMAE interactions at the DFT level were computed with the def2-TZVPP basis set, using counter-poise correction.[67] Ligand docking was performed with AutoDock version 4.2.6,[68,69] with the calculations set up with AutoDockTools version 1.5.6. The crystal structure of the tubulin−MMAE complex (PDB ID 5IYZ)[26] was used as a template. As the binding site is at the interface of chains B and C, other chains, water, and the original ligand (ID 4Q5) were deleted before docking. For the protein, standard Gasteiger charges[70] were used, while for the ligands, restrained electrostatic potential (RESP) charges[71] were computed, based on the TPSSh/def2-TZVPP electron density. All ligand torsion angles, except for the four bonds in the norephedrine moiety, were set to nonrotatable (inactive). A grid box of 40 × 60 × 40 points centered at the original ligand position was calculated with AutoGrid, using default values for other settings. For all ligands, a total of 500 independent search runs utilizing the Lamarckian genetic algorithm,[72] each with a maximum of 2.5 million energy evaluations, were performed; the lowest energy docking pose was in all cases located after 20 search runs.

The DFT calculations were performed with TURBOMOLE versions 7.2 and 7.3,[73−75] the RESP calculations with

DOI: 10.1021/acs.molpharmaceut.9b00437
Mol. Pharmaceutics 2019, 16, 3600−3608

NWChem version 6.8,[76] the coupled cluster calculations with Orca version 4.0.1.2,[77] the SAPT calculations with PSI4 version 1.1,[78] and the noncovalent interaction analysis with NCIplot version 3.[79] Default recommended settings and thresholds were used with the following exceptions: the DFT calculations used the fine m4 grid, except for the vibrational frequencies where the super-fine m5 grid was employed; the coupled cluster calculations were performed with the TightPNO setting. Jmol[80] and VMD[81] were used for visualization.

RESULTS

Shifting the cis/trans Equilibrium. To alter the relative stability of the isomers in solution by structural modification, two main strategies can be employed: (1) modifying the structure so that the interactions between the molecule and the environment, e.g., the solvent, favor one isomer over the other; or (2) modifying the structure so that the intramolecular interactions within the molecule favor one isomer over the other. The nature of the structure modification can be further divided into two, based on if it: (a) stabilizes the active trans-isomer; or (b) destabilizes the inactive cis-isomer.

Naturally, the classes are not mutually exclusive. Any structural modification will exhibit changes in both inter- and intramolecular interactions, and affect both isomers, to some degree.

Modifying the interactions between a drug molecule and its environment will not only affect solute−solvent interactions but will also modify interactions with the drug target. This might be either beneficial or disadvantageous. Tweaking the internal interactions of a molecule will have a lesser effect on the interactions with the binding site. In the present case, where the drug as such works well when in its active conformation, we opt for the strategy of modifying the intramolecular interactions of MMAE and MMAF so that they favor the active trans-conformation over cis.

We recently conducted a combined NMR-spectroscopic and molecular modeling study on the solution properties of MMAE and MMAF.[22] Looking at the three-dimensional structures of the cis and trans-conformers, see Figure 2, one can note some obvious differences between the two conformers. The trans-conformers form an extended structure which corresponds to the tubulin-bound form of the molecule, while the cis-conformers form a more contorted, compact structure that does not fit into the receptor pocket.[22,26,82] Our strategy-of-choice is to shift the conformer equilibrium in favor of the trans-conformers. This implies introducing structural modifications that stabilize the trans-isomer, destabilize the cis-isomer, or a combination of both.

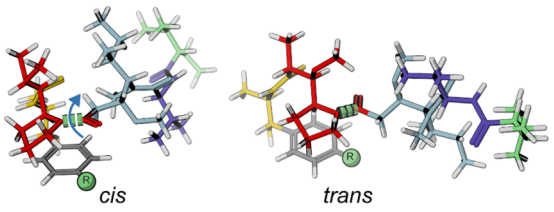

Figure 2. cis and trans-isomers of MMAE. The colors mark the grouping used in the intramolecular energy analysis: Ph (gray), link atoms (yellow), Dap (red), Dil (light blue), Val (purple), and MeVal (green). The site of modification, R, is marked by a green sphere; the blue arrow shows the peptide bond rotation leading to the trans-isomer, and the peptide bond itself is marked by a thick, dashed, green bond.

To properly dissect the interactions between the phenyl group and the rest of the molecule, we performed an analysis using symmetry-adapted perturbation theory for functional groups and intramolecular interactions, F/I-SAPT0.[62−64] Tables 1 and 2 show the interactions for MMAE and MMAF, respectively.

Table 1. Intramolecular Interaction Energies (kJ/mol) between the Terminal Phenyl Group (Ph) and the Four Remaining Amino Acids in the cis and trans-Isomers of MMAE, Grouped by the Type of Interaction

	electrostatic	exchange	induction	dispersion	total
cis					
Ph−Dap	−14.0	+19.9	−5.1	−23.4	−22.6
Ph−Dil	−6.3	+26.9	−2.8	−19.8	−2.0
Ph−Val	−3.0	+1.4	+0.1	−3.7	−5.3
Ph−MeVal	+0.3	+0.0	−0.1	−0.1	+0.1
Ph−All	−23.0	+48.2	−7.9	−47.1	−29.8
trans					
Ph−Dap	−13.2	+37.9	−6.9	−35.2	−17.3
Ph−Dil	−2.9	+0.4	+0.5	−3.3	−5.2
Ph−Val	+0.2	+0.0	+0.1	−0.1	+0.2
Ph−MeVal	−0.1	+0.0	+0.0	−0.0	−0.1
Ph−All	−16.0	+38.4	−6.2	−38.6	−22.4

Table 2. Intramolecular Interaction Energies (kJ/mol) between the Terminal Phenyl Group (Ph) and the Four Remaining Amino Acids in the cis and trans-Isomers of MMAF, Grouped by the Type of Interaction

	electrostatic	exchange	induction	dispersion	total
cis					
Ph−Dap	−13.8	+18.0	−4.6	−21.4	−21.8
Ph−Dil	−5.3	+25.2	−3.2	−20.1	−3.3
Ph−Val	−3.5	+2.7	+0.1	−4.8	−5.5
Ph−MeVal	+0.2	+0.0	−0.1	−0.1	−0.0
Ph−All	−22.4	+45.9	−7.7	−46.4	−30.6
trans					
Ph−Dap	−11.1	+34.6	−6.4	−33.5	−16.5
Ph−Dil	−3.0	+0.4	+0.5	−3.1	−5.2
Ph−Val	+0.1	+0.0	+0.1	−0.1	+0.2
Ph−MeVal	−0.1	+0.0	+0.0	−0.0	−0.1
Ph−All	−14.1	+35.0	−5.8	−36.7	−21.6

The interactions within MMAE and MMAF are nearly twin. Comparing the cis and trans-isomers, we see that the intramolecular interactions between the phenyl and the rest of the molecule are somewhat more favorable in the cis-form. The majority of the total interaction energy comes from interactions between the phenyl (Ph) and the dolaproine (Dap). A closer look at the individual interactions shows, however, that in the cis-form, the interactions between Ph and the dolaisoleuine (Dil) are significant as well, but attractive electrostatic and dispersion interactions are almost completely canceled by the steric repulsion manifested in the exchange interaction. In both isomers, the interactions between Ph and the two valines at the opposite end of the chain are weak. Induction interactions are rather weak overall as well.

Modification of the phenyl ring thus has the potential to tune the intramolecular interactions significantly, and im-

DOI: 10.1021/acs.molpharmaceut.9b00437
Mol. Pharmaceutics 2019, 16, 3600−3608

portantly, in a different manner for the two isomers. To minimize the changes in extramolecular interactions, the modification should in general be small, by some measure. Halogenation is a well-established strategy in drug development, and a significant portion of the drugs on the market contain fluorine and/or chlorine.[83−86] Furthermore, halogenation should have an immediate effect on all of the important intramolecular interactions. A priori, one could expect dispersion interactions to become stronger, especially for chlorinated species. This effect could be offset by a possible increase in steric exchange repulsion due to the larger size of the halogens, at least if the geometry otherwise stays constant. Providing an educated guess for the change in electrostatic interactions arising from the substitutions is more difficult, as there will be a significant redistribution of charge due to the electron-withdrawing halogens. Fortunately, all of the induced changes can be tracked with the F/I-SAPT0 method, rendering guesswork a stimulating but superfluous activity.

Here, we opt for substituting one of the five hydrogens of the terminal phenyl group by either fluorine or chlorine. Exploratory modeling at the DFT level found methyl substitution to be inferior to halogenation, and that substitution at the meta position favors the cis-isomer, see Table S1 in the Supporting Information. Furthermore, while the rotation around the phenyl C−C bond is reasonably fast in solution, this might not be the case when bound to tubulin. Thus, substitution at the meta and ortho positions would double the number of isomers to be considered, exacerbating the conformer issue. Another aspect favoring substitutions in the para-position is that it represents a feasible synthetic route for modification.

Table 3 shows the energy difference between the cis and trans forms of MMAE, MMAF, and their halogenated analogues, computed at the CCSD(T) level, in a simulated water medium at 37 °C (see Methods for details), as well as the available experimental data;[22] we note that computing the thermal corrections at 295 and 310 K results in the same simulated relative energies for MMAE and MMAF.

Table 3. Energy Differences (kJ/mol) between the cis and trans-Isomers of the Studied Auristatins[a]

	cis−trans energy difference (cis/trans ratio)		
molecule	Δ*H*, 310 K	Δ*G*, 310 K	Δ*G*, 295 K, exp
MMAE	+1.0 (59:41)	+1.3 (62:38)	+0.9 (59:41)
para-F-MMAE	−4.0 (17:83)	−3.4 (21:79)	
para-Cl-MMAE	−1.2 (39:61)	−0.3 (47:53)	
MMAF	−0.1 (49:51)	−0.2 (48:52)	+0.5 (55:45)
para-F-MMAF	−7.0 (6:94)	−5.6 (10:90)	
para-Cl-MMAF	−7.4 (5:95)	−7.2 (6:94)	

[a]The energies of the cis-isomers are set to zero, so a negative value indicates that the specific trans-isomer is lower in energy (Boltzmann ratios within parentheses). Computed at the DLPNO-CCSD(T)/def2-[T,Q]ZVPPD/COSMO level.

As a side note, a comparison to the relative energies computed at the DFT level (Table S1) underlines the importance of using a highly accurate level of theory for computing the isomer distribution. For both MMAE and MMAF, the DFT calculations unduly favor the cis-isomer by 6 kJ/mol, thus predicting cis/trans-isomer ratios of 94:6 and 91:9 for MMAE and MMAF, respectively.

Chlorination of MMAE has a rather small effect on the cis/trans ratio. The three other halogenations shift the equilibrium significantly toward the preferred trans-isomer. The most promising results are seen for chlorinated MMAF, where the computed cis/trans ratio is 6:94. Compared to pure MMAF, the amount of problematic cis-isomer is thus reduced to a tenth.

Table 4 shows a summary of the F/I-SAPT0 analysis of the changes in intramolecular interactions between the terminal phenyl group and the Dap and Dil residues upon halogenation for MMAE and MMAF.

From the data in Table 4, one can note a common feature: halogenation always decreases the intramolecular attraction within the cis-isomers, while the interactions within the trans-isomer become more favorable. This is the main driving force for the shift toward the trans-isomer upon halogenation at the para-position of the phenyl group in both MMAE and MMAF.

The individual components of the interaction energies also show some common features. In all cis-isomers, the electrostatic attraction is decreased (but stays attractive), while the trans-isomers experience an enhanced electrostatic attraction. For the steric exchange repulsion, the situation is reversed, with the halogenated cis-forms consistently having less steric repulsion than their unsubstituted counterparts, despite the larger size of the halogens compared to hydrogen.

For the chlorinated species, dispersion interactions are, as expected, enhanced. This is also clearly evident in the noncovalent interaction (NCI) analysis. NCI analysis reveals regions in the molecule where weak interactions like dispersion are manifested, based on various properties of the electron density,[79,87] and is known to work well for halogenated species.[88] Figure 3 shows the NCIplot in real-space for MMAE and Cl-MMAE; the expansion of the region of dispersion interactions is rather notable, now extending further from the phenyl−pyrrolidine stacking interaction.

For the fluorinated species, changes in the dispersion interactions are damped compared to their chlorinated counterparts, and in the case of the cis-isomer, dispersion actually decreases. Thus, while the general trends of the changes perhaps could be predicted a priori, the relative magnitudes, and sometimes even the direction of the adjustment require rigorous quantum chemical studies.

Interaction with Tubulin. In the previous section, we identified two, maybe three promising candidates for improved auristatins, based on the criterion that the biologically active trans-isomer should be dominant. In decreasing order of potency, these are the para-substituted Cl-MMAF, F-MMAF, and F-MMAE, with predicted portions of 94, 90, and 79% trans-isomer in solution, respectively, compared to the 38 and 52% of the original, unsubstituted MMAE and MMAF. A more favorable cis/trans ratio is in itself not enough, however. The new molecules have to perform well also in their therapeutic function of binding to the tubulins.

Although halogenation was chosen as a minimally intrusive chemical modification from the extramolecular standpoint, some changes in the interactions with the environment are always to be expected. The simulated changes in solvation free energy are +1.9, +1.4, and +1.4 kJ/mol for the trans-conformations of Cl-MMAF, F-MMAF, and F-MMAE, respectively, that is, slightly less soluble in water. Changing the dielectric constant from 78 to 32.6, simulating methanol, or alternatively, the lower dielectricity inside cells,[89,90] changes the relative solvation energies by at most 0.1 kJ/mol. Overall,

DOI: 10.1021/acs.molpharmaceut.9b00437
Mol. Pharmaceutics 2019, 16, 3600−3608

Table 4. Interaction Energy Differences (kJ/mol) between Halogenated and Unsubstituted MMAE and MMAF[a]

	MMAE				MMAF			
halogen, isomer	elst.	exch.	disp.	total	elst.	exch.	disp.	total
F, cis								
Ph−Dap	+8.3	−3.7	+1.9	+7.6	+7.8	−1.4	+0.7	+7.5
Ph−Dil	+2.7	−5.2	+2.0	+0.1	+0.9	+0.5	−0.6	+0.9
Ph−All	+10.3	−9.6	+4.6	**+6.9**	+7.6	−1.3	+0.2	**+7.0**
F, trans								
Ph−Dap	−5.7	+1.7	−1.5	−5.3	−5.7	+2.0	−1.9	−5.4
Ph−Dil	+0.7	+0.9	−1.0	+0.2	+0.6	+1.0	−1.2	+0.0
Ph−All	−4.9	+2.6	−2.6	**−4.9**	−5.0	+3.0	−3.1	**−5.3**
Cl, cis								
Ph−Dap	+7.5	+0.7	−4.2	+4.0	+7.1	+1.8	−5.2	+3.6
Ph−Dil	+0.9	−0.8	−1.3	−1.1	+0.1	−0.5	−0.8	−0.7
Ph−All	+7.7	−0.9	−5.0	**+2.0**	+6.8	−0.4	−4.8	**+1.9**
Cl, trans								
Ph−Dap	−5.4	−1.1	−3.7	−10.2	−5.8	−0.4	−4.2	−10.5
Ph−Dil	−0.6	+6.3	−4.9	+0.4	−0.4	+5.9	−4.7	+0.4
Ph−All	−5.8	+5.3	−8.7	**−9.6**	−5.9	+5.4	−8.9	**−9.9**

[a]Negative values indicate that the halogenation lowers the energy. The "total" interaction energies include induction terms and the "Ph−All" terms include contributions from the valines.

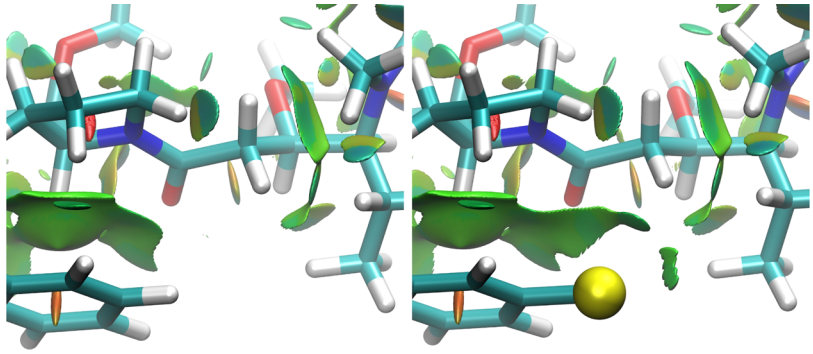

Figure 3. Plot of noncovalent interactions in the trans-conformations of MMAE (left) and Cl-MMAE (right). Green areas depict dispersion interactions within the molecules.

the solvation energy differences are very small, indicating small changes also in the interaction with other molecules and moieties like the tubulin binding pocket.

To more directly estimate the binding energy for the modified auristatins, we constructed a model of the binding pocket, using the crystal structure PDB ID 5IYZ[26] as a starting point. The model includes the MMAE ligand and the residues within 5 Å from the para-hydrogen of the C-terminal phenyl, that is, Gln-11, Gln-15, Lys-19, Tyr-224, Gly-225, Asn-228, and the guanosine diphosphate 501, as well as 8 of the closest crystal waters, in total 293 atoms, see Figure 4. The model thus includes the most important residues that would experience and exert modified interactions with the ligand due to halogenation. The structural difference between MMAE and MMAF, that is, the difference between norephedrine and phenylalanine, lies five bonds away from the site of modification. Therefore, the assumption that the change in interaction energies upon halogenation will be very similar for MMAE and MMAF should be a good first approximation, even if distant ligand substitutions can have a non-negligible effect on intermolecular interactions.[91] Ideally, an even larger model of the binding site, where also residues surrounding the −OH/−COOH groups of MMAE/MMAF are included would be employed; this would lead to an inordinate model system size, however.

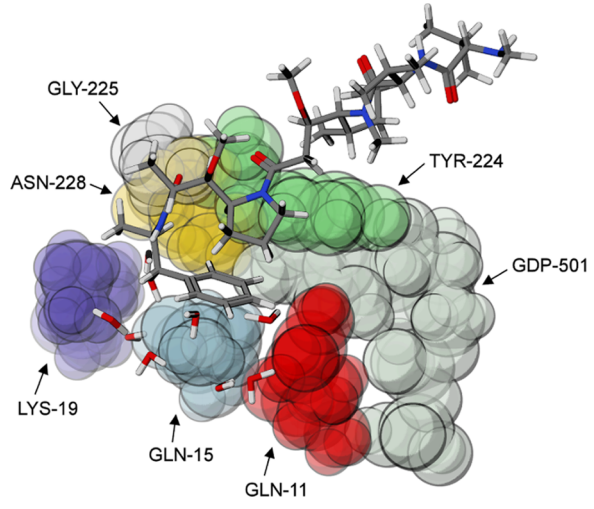

Figure 4. Model of MMAE bound to tubulin. The structures of MMAE and the water molecules are shown as stick models, and the closest amino acids and the guanosine diphosphate are shown as colored space-filling spheres.

DOI: 10.1021/acs.molpharmaceut.9b00437
Mol. Pharmaceutics 2019, 16, 3600−3608

At the F/I-SAPT0 level, the interaction energy differences are comparable to the differences in solvation energy, with the F-MMAE and Cl-MMAE interaction energies decreased by 0.3 and 2.0 kJ/mol, respectively.

Dispersion-corrected DFT interaction energies corroborate these findings: at the TPSSh-D3 level, F-MMAE and Cl-MMAE interactions with the tubulin model are weaker by 0.6 and 1.7 kJ/mol respectively, compared to the unmodified MMAE. Looking at total binding energies from the model, that is, using relaxed MMAE structures, the binding is slightly less favorable for the halogenated species, with binding free energy weaker by 4.1 and 4.4 kJ/mol for F-MMAE and Cl-MMAE, respectively. This can be traced to the interference of the tyrosine residue (Tyr-224, see Figure 4) which functions as a wedge, separating the terminal phenyl from the pyrrolidine. The increase in the stability of the halogenated trans-isomers that springs from the increased favorable intramolecular interactions are thus dampened upon tubulin binding. Thus, while the actual binding strength, measured as the direct interaction energy between the ligand and the binding site, is almost unaffected, the computed binding free energy is somewhat weaker.

We duly note that the molecular model used for computing the drug−tubulin interaction will have a non-negligible effect on the binding energy. Here, we chose a model as large as possible, considering computing capability. To keep the tubulin frame of the model in close correspondence to the experimental structure, some surface atoms require fixing to their crystallographic positions; also, the positions of the H_2O oxygens were fixed to restrict their movement away from the binding site. As the positions of the amino acids in the binding pocket have been constrained based on the crystal structure of the unsubstituted MMAE/tubulin complex, there might be a slight bias against the halogenated species, as the halogens naturally are somewhat larger than the hydrogen they replace.

We also performed a simulated molecular docking study of MMAE, F-MMAE, and Cl-MMAE to tubulin, using the AutoDock protocol (see Methods). Docking models naturally have their own limitations,[92] but do provide a complementary view on the binding affinity. The experimental docking pose[26] was located as the minimum for MMAE, and the halogenated derivatives were docked in a near-identical manner. The minimum energy docking position for both F-MMAE and Cl-MMAE was found to bind minutely weaker, by 1.1 kJ/mol. The predicted mean binding energy was also slightly lower, by 1.5 and 1.8 kJ/mol for F-MMAE and Cl-MMAE, respectively. Also here, a slight bias toward the original MMAE is possible, as the binding pocket was fixed to the crystal structure.

The binding affinity of a drug molecule is of course very sensitive to the interaction energy between the drug and its target. Using the simple $\Delta G = -RT\ln(K_d)$ relation, a $\Delta\Delta G$ of 6 kJ/mol changes the binding affinity by an order of magnitude. At a minimum, the simple exploration presented in this section gives no reason for concern regarding the binding of the modified drugs. This is especially true for the halogenated MMAF derivatives, as MMAF in itself is known to bind 5 times stronger to the tubulins compared to MMAE.[26]

CONCLUSIONS

The cytotoxic auristatins are widely used warheads in modern ADCs. They do, however, suffer from a potentially serious flaw: in solution, half of the drug molecules exist, temporarily, in their biologically inactive cis-conformation. This raises a number of concerns regarding their safety and efficacy. The active trans-isomer will, after its release in the cancer cell, quickly bind to tubulin, causing apoptosis, while the cis-form remains inactive. The cis-isomer will, eventually, also activate by transforming into the trans-form; this activation might, however, come too late, when the drug molecule has already escaped the confines of the target cell into healthy tissue.

The existence of two distinct isomers also suggests an immediate route for developing improved derivatives. Herein, we have focused on the rational design of novel auristatin derivatives which would favor the biologically active trans-conformation. By performing a careful quantum chemical investigation of the intramolecular forces governing the cis/trans equilibrium, we have identified candidates for improved cancer therapeutics. High-level coupled cluster calculations suggest that a halogen substitution at the para-position of the C-terminal phenyl ring in MMAE and MMAF leads to significantly more favorable isomer ratios. The most promising candidates are the chlorinated and fluorinated MMAF derivatives, which are predicted to shift the trans ratio to 94 and 90%, respectively. In terms of ADC research, this suggests that with these improved warheads the administrated doses could be reduced by 40−50% without affecting the efficacy of the ADCs. A decrease in the required drug dosage is in itself advantageous. From another point of view, the amount of potentially harmful cis-isomer administered is reduced significantly.

Presently, it is naturally impossible to ascertain whether these simple halogenated derivatives will proceed all the way through clinical trials, or if the candidates will require additional tuning of their properties. Nevertheless, we have shown that the amount of the temporarily inactive cis-form of the auristatins can be addressed already at the computational drug design stage. Furthermore, the modifications have been designed with synthetic feasibility and tubulin binding interactions in mind.

In general, tuning the conformational equilibrium offers a new, complementary avenue for reaching improved auristatin-based cancer pharmaceuticals to those currently pursued in the scientific literature.

ASSOCIATED CONTENT

Supporting Information

The Supporting Information is available free of charge on the ACS Publications website at DOI: 10.1021/acs.molpharmaceut.9b00437.

Isomer energy differences computed at the DFT level; atomic coordinates of modified auristatins and auristatin/tubulin models; definition of fixed atoms; AutoDock PDBQT ligand files (PDF)

AUTHOR INFORMATION

Corresponding Author

*E-mail: mikael.johansson@helsinki.fi.

ORCID

Iris K. Sokka: 0000-0002-5148-4987
Filip S. Ekholm: 0000-0002-4461-2215
Mikael P. Johansson: 0000-0002-9793-8235

Notes

The authors declare no competing financial interest.

DOI: 10.1021/acs.molpharmaceut.9b00437
Mol. Pharmaceutics 2019, 16, 3600−3608

■ ACKNOWLEDGMENTS

CSC-The Finnish IT Center for Science and the Finnish Grid and Cloud Infrastructure (urn:nbn:fi:research-infras-2016072533) provided ample computer time. This work has been supported by the Academy of Finland (projects 289179 and 319453), Jane and Aatos Erkko Foundation, Waldemar von Frenckells stiftelse, and University of Helsinki research funds.

■ REFERENCES

(1) Bai, R.; Pettit, G. R.; Hamel, E. Dolastatin 10, a Powerful Cytostatic Peptide Derived from a Marine Animal. *Biochem. Pharmacol.* **1990**, *39*, 1941−1949.
(2) Wu, A. M.; Senter, P. D. Arming Antibodies: Prospects and Challenges for Immunoconjugates. *Nat. Biotechnol.* **2005**, *23*, 1137−1146.
(3) Doronina, S. O.; Mendelsohn, B. A.; Bovee, T. D.; Cerveny, C. G.; Alley, S. C.; Meyer, D. L.; Oflazoglu, E.; Toki, B. E.; Sanderson, R. J.; Zabinski, R. F.; et al. Enhanced Activity of Monomethylauristatin F through Monoclonal Antibody Delivery: Effects of Linker Technology on Efficacy and Toxicity. *Bioconjugate Chem.* **2006**, *17*, 114−124.
(4) Senter, P. D.; Sievers, E. L. The Discovery and Development of Brentuximab Vedotin for Use in Relapsed Hodgkin Lymphoma and Systemic Anaplastic Large Cell Lymphoma. *Nat. Biotechnol.* **2012**, *30*, 631−637.
(5) Chen, H.; Lin, Z.; Arnst, K.; Miller, D.; Li, W. Tubulin Inhibitor-Based Antibody-Drug Conjugates for Cancer Therapy. *Molecules* **2017**, *22*, No. 1281.
(6) Schrama, D.; Reisfeld, R. A.; Becker, J. C. Antibody Targeted Drugs as Cancer Therapeutics. *Nat. Rev. Drug Discovery* **2006**, *5*, 147−159.
(7) Mullard, A. Maturing Antibody−Drug Conjugate Pipeline Hits 30. *Nat. Rev. Drug Discovery* **2013**, *12*, 329−332.
(8) Diamantis, N.; Banerji, U. Antibody-Drug Conjugates—an Emerging Class of Cancer Treatment. *Br. J. Cancer* **2016**, *114*, 362−367.
(9) Lucas, A.; Price, L.; Schorzman, A.; Storrie, M.; Piscitelli, J.; Razo, J.; Zamboni, W. Factors Affecting the Pharmacology of Antibody−Drug Conjugates. *Antibodies* **2018**, *7*, 10.
(10) Lu, Z.-R.; Qiao, P. Drug Delivery in Cancer Therapy, Quo Vadis? *Mol. Pharmceutics* **2018**, *15*, 3603−3616.
(11) Alberts, B.; Johnson, A. D.; Lewis, J.; Morgan, D.; Raff, M.; Roberts, K.; Walter, P. *Molecular Biology of the Cell*, 6th ed.; Garland Science, Taylor & Francis Group: New York, NY, 2015.
(12) Kovtun, Y. V.; Goldmacher, V. S. Cell Killing by Antibody−Drug Conjugates. *Cancer Lett.* **2007**, *255*, 232−240.
(13) Ehrlich, P. Experimental Researches on Specific Therapy: On Immunity with Special Reference to the Relationship between Distribution and Action of Antigens. First Harben Lecture (1907). In *The Collected Papers of Paul Ehrlich*; Elsevier, 1960; pp 106−117.
(14) Ehrlich, P. Address in Pathology, ON CHEMIOTHERAPY: Delivered before the Seventeenth International Congress of Medicine. *Br. Med. J.* **1913**, *2*, 353−359.
(15) Albert, A. Selective Toxicity. *Nature* **1950**, *165*, 12−16.
(16) Schwartz, R. S. Paul Ehrlich's Magic Bullets. *N. Engl. J. Med.* **2004**, *350*, 1079−1080.
(17) Winau, F.; Westphal, O.; Winau, R. Paul Ehrlich — in Search of the Magic Bullet. *Microbes Infect.* **2004**, *6*, 786−789.
(18) Lewis, L. D. Cancer Pharmacotherapy: 21st Century "magic Bullets" and Changing Paradigms. *Br. J. Clin. Pharmacol.* **2006**, *62*, 1−4.
(19) Bosch, F.; Rosich, L. The Contributions of Paul Ehrlich to Pharmacology: A Tribute on the Occasion of the Centenary of His Nobel Prize. *Pharmacology* **2008**, *82*, 171−179.
(20) Strebhardt, K.; Ullrich, A. Paul Ehrlich's Magic Bullet Concept: 100 Years of Progress. *Nat. Rev. Cancer* **2008**, *8*, 473−480.
(21) Lambert, J. M. Antibody−Drug Conjugates (ADCs): Magic Bullets at Last! *Mol. Pharmceutics* **2015**, *12*, 1701−1702.
(22) Johansson, M. P.; Maaheimo, H.; Ekholm, F. S. New Insight on the Structural Features of the Cytotoxic Auristatins MMAE and MMAF Revealed by Combined NMR Spectroscopy and Quantum Chemical Modelling. *Sci. Rep.* **2017**, *7*, No. 15920.
(23) Okeley, N. M.; Miyamoto, J. B.; Zhang, X.; Sanderson, R. J.; Benjamin, D. R.; Sievers, E. L.; Senter, P. D.; Alley, S. C. Intracellular Activation of SGN-35, a Potent Anti-CD30 Antibody-Drug Conjugate. *Clin. Cancer Res.* **2010**, *16*, 888−897.
(24) Donaghy, H. Effects of Antibody, Drug and Linker on the Preclinical and Clinical Toxicities of Antibody-Drug Conjugates. *mAbs* **2016**, *8*, 659−671.
(25) Lambert, J. M.; Morris, C. Q. Antibody−Drug Conjugates (ADCs) for Personalized Treatment of Solid Tumors: A Review. *Adv. Ther.* **2017**, *34*, 1015−1035.
(26) Waight, A. B.; Bargsten, K.; Doronina, S.; Steinmetz, M. O.; Sussman, D.; Prota, A. E. Structural Basis of Microtubule Destabilization by Potent Auristatin Anti-Mitotics. *PLoS ONE* **2016**, *11*, No. e0160890.
(27) Ekholm, F.; Ruokonen, S.-K.; Redón, M.; Pitkänen, V.; Vilkman, A.; Saarinen, J.; Helin, J.; Satomaa, T.; Wiedmer, S. Hydrophilic Monomethyl Auristatin E Derivatives as Novel Candidates for the Design of Antibody-Drug Conjugates. *Separations* **2019**, *6*, 1.
(28) Miyazaki, K.; Kobayashi, M.; Natsume, T.; Gondo, M.; Mikami, T.; Sakakibara, K.; Tsukagoshi, S. Synthesis and Antitumor Activity of Novel Dolastatin 10 Analogs. *Chem. Pharm. Bull.* **1995**, *43*, 1706−1718.
(29) Doronina, S. O.; Toki, B. E.; Torgov, M. Y.; Mendelsohn, B. A.; Cerveny, C. G.; Chace, D. F.; DeBlanc, R. L.; Gearing, R. P.; Bovee, T. D.; Siegall, C. B.; et al. Development of Potent Monoclonal Antibody Auristatin Conjugates for Cancer Therapy. *Nat. Biotechnol.* **2003**, *21*, 778−784.
(30) Burns, K. E.; Robinson, M. K.; Thévenin, D. Inhibition of Cancer Cell Proliferation and Breast Tumor Targeting of PHLIP−Monomethyl Auristatin E Conjugates. *Mol. Pharmaceutics* **2015**, *12*, 1250−1258.
(31) Maderna, A.; Leverett, C. A. Recent Advances in the Development of New Auristatins: Structural Modifications and Application in Antibody Drug Conjugates. *Mol. Pharmaceutics* **2015**, *12*, 1798−1812.
(32) Lhospice, F.; Brégeon, D.; Belmant, C.; Dennler, P.; Chiotellis, A.; Fischer, E.; Gauthier, L.; Boëdec, A.; Rispaud, H.; Savard-Chambard, S.; et al. Site-Specific Conjugation of Monomethyl Auristatin E to Anti-CD30 Antibodies Improves Their Pharmacokinetics and Therapeutic Index in Rodent Models. *Mol. Pharmaceutics* **2015**, *12*, 1863−1871.
(33) Cunningham, D.; Parajuli, K. R.; Zhang, C.; Wang, G.; Mei, J.; Zhang, Q.; Liu, S.; You, Z. Monomethyl Auristatin E Phosphate Inhibits Human Prostate Cancer Growth: MMAEp Inhibits Prostate Cancer. *The Prostate* **2016**, *76*, 1420−1430.
(34) Ekholm, F. S.; Pynnönen, H.; Vilkman, A.; Pitkänen, V.; Helin, J.; Saarinen, J.; Satomaa, T. Introducing Glycolinkers for the Functionalization of Cytotoxic Drugs and Applications in Antibody-Drug Conjugation Chemistry. *ChemMedChem* **2016**, *11*, 2501−2505.
(35) Dugal-Tessier, J.; Barnscher, S. D.; Kanai, A.; Mendelsohn, B. A. Synthesis and Evaluation of Dolastatin 10 Analogues Containing Heteroatoms on the Amino Acid Side Chains. *J. Nat. Prod.* **2017**, *80*, 2484−2491.
(36) Mendelsohn, B. A.; Barnscher, S. D.; Snyder, J. T.; An, Z.; Dodd, J. M.; Dugal-Tessier, J. Investigation of Hydrophilic Auristatin Derivatives for Use in Antibody Drug Conjugates. *Bioconjugate Chem.* **2017**, *28*, 371−381.
(37) Shi, B.; Wu, M.; Li, Z.; Xie, Z.; Wei, X.; Fan, J.; Xu, Y.; Ding, D.; Akash, S. H.; Chen, S.; et al. Antitumor Activity of a 5T4 Targeting Antibody Drug Conjugate with a Novel Payload Derived from MMAF via C-Lock Linker. *Cancer Med.* **2019**, *8*, 1793−1805.
(38) Ryde, U.; Söderhjelm, P. Ligand-Binding Affinity Estimates Supported by Quantum-Mechanical Methods. *Chem. Rev.* **2016**, *116*, 5520−5566.

DOI: 10.1021/acs.molpharmaceut.9b00437
Mol. Pharmaceutics 2019, 16, 3600−3608

(39) Ehrlich, S.; Göller, A. H.; Grimme, S. Towards Full Quantum-Mechanics-Based Protein-Ligand Binding Affinities. *ChemPhysChem* **2017**, *18*, 898−905.
(40) Hawkins, P. C. D. Conformation Generation: The State of the Art. *J. Chem. Inf. Model.* **2017**, *57*, 1747−1756.
(41) Caldararu, O.; Olsson, M. A.; Riplinger, C.; Neese, F.; Ryde, U. Binding Free Energies in the SAMPL5 Octa-Acid Host−Guest Challenge Calculated with DFT-D3 and CCSD(T). *J. Comput.-Aided Mol. Des.* **2017**, *31*, 87−106.
(42) Steinmann, C.; Olsson, M. A.; Ryde, U. Relative Ligand-Binding Free Energies Calculated from Multiple Short QM/MM MD Simulations. *J. Chem. Theory Comput.* **2018**, *14*, 3228−3237.
(43) von Lilienfeld, O. A. Quantum Machine Learning in Chemical Compound Space. *Angew. Chem., Int. Ed.* **2018**, *57*, 4164−4169.
(44) Amaro, R. E.; Mulholland, A. J. Multiscale Methods in Drug Design Bridge Chemical and Biological Complexity in the Search for Cures. *Nat. Rev. Chem.* **2018**, *2*, No. 0148.
(45) Cavasin, A. T.; Hillisch, A.; Uellendahl, F.; Schneckener, S.; Göller, A. H. Reliable and Performant Identification of Low-Energy Conformers in the Gas Phase and Water. *J. Chem. Inf. Model.* **2018**, *58*, 1005−1020.
(46) Cole, D. J.; Cabeza de Vaca, I.; Jorgensen, W. L. Computation of Protein−Ligand Binding Free Energies Using Quantum Mechanical Bespoke Force Fields. *Med. Chem. Commun.* **2019**. DOI: 10.1039/C9MD00017H
(47) Kohn, W. Nobel Lecture: Electronic Structure of Matter—Wave Functions and Density Functionals. *Rev. Mod. Phys.* **1999**, *71*, 1253−1266.
(48) Staroverov, V. N.; Scuseria, G. E.; Tao, J.; Perdew, J. P. Comparative Assessment of a New Nonempirical Density Functional: Molecules and Hydrogen-Bonded Complexes. *J. Chem. Phys.* **2003**, *119*, 12129−12137.
(49) Grimme, S.; Antony, J.; Ehrlich, S.; Krieg, H. A Consistent and Accurate *Ab Initio* Parametrization of Density Functional Dispersion Correction (DFT-D) for the 94 Elements H-Pu. *J. Chem. Phys.* **2010**, *132*, No. 154104.
(50) Becke, A. D.; Johnson, E. R. A Density-Functional Model of the Dispersion Interaction. *J. Chem. Phys.* **2005**, *123*, No. 154101.
(51) Grimme, S.; Ehrlich, S.; Goerigk, L. Effect of the Damping Function in Dispersion Corrected Density Functional Theory. *J. Comput. Chem.* **2011**, *32*, 1456−1465.
(52) Weigend, F.; Ahlrichs, R. Balanced Basis Sets of Split Valence, Triple Zeta Valence and Quadruple Zeta Valence Quality for H to Rn: Design and Assessment of Accuracy. *Phys. Chem. Chem. Phys.* **2005**, *7*, 3297.
(53) Klamt, A.; Schüürmann, G. COSMO: A New Approach to Dielectric Screening in Solvents with Explicit Expressions for the Screening Energy and Its Gradient. *J. Chem. Soc., Perkin Trans. 2* **1993**, 799−805.
(54) Riplinger, C.; Neese, F. An Efficient and near Linear Scaling Pair Natural Orbital Based Local Coupled Cluster Method. *J. Chem. Phys.* **2013**, *138*, No. 034106.
(55) Riplinger, C.; Sandhoefer, B.; Hansen, A.; Neese, F. Natural Triple Excitations in Local Coupled Cluster Calculations with Pair Natural Orbitals. *J. Chem. Phys.* **2013**, *139*, No. 134101.
(56) Riplinger, C.; Pinski, P.; Becker, U.; Valeev, E. F.; Neese, F. Sparse Maps—A Systematic Infrastructure for Reduced-Scaling Electronic Structure Methods. II. Linear Scaling Domain Based Pair Natural Orbital Coupled Cluster Theory. *J. Chem. Phys.* **2016**, *144*, No. 024109.
(57) Halkier, A.; Helgaker, T.; Jørgensen, P.; Klopper, W.; Koch, H.; Olsen, J.; Wilson, A. K. Basis-Set Convergence in Correlated Calculations on Ne, N_2, and H_2O. *Chem. Phys. Lett.* **1998**, *286*, 243−252.
(58) Rappoport, D.; Furche, F. Property-Optimized Gaussian Basis Sets for Molecular Response Calculations. *J. Chem. Phys.* **2010**, *133*, No. 134105.
(59) Liakos, D. G.; Sparta, M.; Kesharwani, M. K.; Martin, J. M. L.; Neese, F. Exploring the Accuracy Limits of Local Pair Natural Orbital Coupled-Cluster Theory. *J. Chem. Theory Comput.* **2015**, *11*, 1525−1539.
(60) Liakos, D. G.; Neese, F. Is It Possible To Obtain Coupled Cluster Quality Energies at near Density Functional Theory Cost? Domain-Based Local Pair Natural Orbital Coupled Cluster vs Modern Density Functional Theory. *J. Chem. Theory Comput.* **2015**, *11*, 4054−4063.
(61) Lassfolk, R.; Rahkila, J.; Johansson, M. P.; Ekholm, F. S.; Wärnå, J.; Leino, R. Acetyl Group Migration Across the Saccharide Units in Oligomannoside Model Compound. *J. Am. Chem. Soc.* **2019**, *141*, 1646−1654.
(62) Jeziorski, B.; Moszynski, R.; Szalewicz, K. Perturbation Theory Approach to Intermolecular Potential Energy Surfaces of van Der Waals Complexes. *Chem. Rev.* **1994**, *94*, 1887−1930.
(63) Parrish, R. M.; Parker, T. M.; Sherrill, C. D. Chemical Assignment of Symmetry-Adapted Perturbation Theory Interaction Energy Components: The Functional-Group SAPT Partition. *J. Chem. Theory Comput.* **2014**, *10*, 4417−4431.
(64) Parrish, R. M.; Gonthier, J. F.; Corminbœuf, C.; Sherrill, C. D. Communication: Practical Intramolecular Symmetry Adapted Perturbation Theory via Hartree-Fock Embedding. *J. Chem. Phys.* **2015**, *143*, No. 051103.
(65) Löwdin, P.-O. Twenty-Five Years of Sanibel Symposia: A Brief Historic and Scientific Survey. *Int. J. Quantum Chem., Quantum Chem. Symp.* **1986**, *28*, 19−37.
(66) Papajak, E.; Zheng, J.; Xu, X.; Leverentz, H. R.; Truhlar, D. G. Perspectives on Basis Sets Beautiful: Seasonal Plantings of Diffuse Basis Functions. *J. Chem. Theory Comput.* **2011**, *7*, 3027−3034.
(67) Boys, S. F.; Bernardi, F. The Calculation of Small Molecular Interactions by the Differences of Separate Total Energies. Some Procedures with Reduced Errors. *Mol. Phys.* **1970**, *19*, 553−566.
(68) Huey, R.; Morris, G. M.; Olson, A. J.; Goodsell, D. S. A Semiempirical Free Energy Force Field with Charge-Based Desolvation. *J. Comput. Chem.* **2007**, *28*, 1145−1152.
(69) Morris, G. M.; Huey, R.; Lindstrom, W.; Sanner, M. F.; Belew, R. K.; Goodsell, D. S.; Olson, A. J. AutoDock4 and AutoDockTools4: Automated Docking with Selective Receptor Flexibility. *J. Comput. Chem.* **2009**, *30*, 2785−2791.
(70) Gasteiger, J.; Marsili, M. Iterative Partial Equalization of Orbital Electronegativity—a Rapid Access to Atomic Charges. *Tetrahedron* **1980**, *36*, 3219−3228.
(71) Bayly, C. I.; Cieplak, P.; Cornell, W.; Kollman, P. A. A Well-Behaved Electrostatic Potential Based Method Using Charge Restraints for Deriving Atomic Charges: The RESP Model. *J. Phys. Chem. A* **1993**, *97*, 10269−10280.
(72) Morris, G. M.; Goodsell, D. S.; Halliday, R. S.; Huey, R.; Hart, W. E.; Belew, R. K.; Olson, A. J. Automated Docking Using a Lamarckian Genetic Algorithm and an Empirical Binding Free Energy Function. *J. Comput. Chem.* **1998**, *19*, 1639−1662.
(73) *Turbomole V7.2*, a Development of University of Karlsruhe and Forschungszentrum Karlsruhe GmbH, 1989−2007; TURBOMOLE GmbH, since 2007. http://www.turbomole.com, 2017.
(74) Ahlrichs, R.; Bär, M.; Häser, M.; Horn, H.; Kölmel, C. Electronic Structure Calculations on Workstation Computers: The Program System Turbomole. *Chem. Phys. Lett.* **1989**, *162*, 165−169.
(75) Eichkorn, K.; Weigend, F.; Treutler, O.; Ahlrichs, R. Auxiliary Basis Sets for Main Row Atoms and Transition Metals and Their Use to Approximate Coulomb Potentials. *Theor. Chem. Acc.* **1997**, *97*, 119−124.
(76) Valiev, M.; Bylaska, E. J.; Govind, N.; Kowalski, K.; Straatsma, T. P.; Van Dam, H. J. J.; Wang, D.; Nieplocha, J.; Apra, E.; Windus, T. L.; et al. NWChem: A Comprehensive and Scalable Open-Source Solution for Large Scale Molecular Simulations. *Comput. Phys. Commun.* **2010**, *181*, 1477−1489.
(77) Neese, F. The ORCA Program System. *Wiley Interdiscip. Rev.: Comput. Mol. Sci.* **2012**, *2*, 73−78.
(78) Parrish, R. M.; Burns, L. A.; Smith, D. G. A.; Simmonett, A. C.; DePrince, A. E.; Hohenstein, E. G.; Bozkaya, U.; Sokolov, A. Y.; Di Remigio, R.; Richard, R. M.; et al. PSI4 1.1: An Open-Source

DOI: 10.1021/acs.molpharmaceut.9b00437
Mol. Pharmaceutics 2019, 16, 3600−3608

Electronic Structure Program Emphasizing Automation, Advanced Libraries, and Interoperability. *J. Chem. Theory Comput.* **2017**, *13*, 3185−3197.
(79) Contreras-García, J.; Johnson, E. R.; Keinan, S.; Chaudret, R.; Piquemal, J.-P.; Beratan, D. N.; Yang, W. NCIPLOT: A Program for Plotting Noncovalent Interaction Regions. *J. Chem. Theory Comput.* **2011**, *7*, 625−632.
(80) Jmol: An Open-Source Java Viewer for Chemical Structures in 3D. http://www.jmol.org/.
(81) Humphrey, W.; Dalke, A.; Schulten, K. VMD: Visual Molecular Dynamics. *J. Mol. Graphics* **1996**, *14*, 33−38.
(82) Wang, Y.; Benz, F. W.; Wu, Y.; Wang, Q.; Chen, Y.; Chen, X.; Li, H.; Zhang, Y.; Zhang, R.; Yang, J. Structural Insights into the Pharmacophore of Vinca Domain Inhibitors of Microtubules. *Mol. Pharmacol.* **2016**, *89*, 233−242.
(83) Naumann, K. Influence of chlorine substituents on biological activity of chemicals. *J. Prakt. Chem.* **1999**, *341*, 417−435.
(84) Hernandes, M.; Cavalcanti, S. M.; Moreira, D. R.; de Azevedo Junior, W.; Leite, A. C. Halogen Atoms in the Modern Medicinal Chemistry: Hints for the Drug Design. *Curr. Drug Targets* **2010**, *11*, 303−314.
(85) Gillis, E. P.; Eastman, K. J.; Hill, M. D.; Donnelly, D. J.; Meanwell, N. A. Applications of Fluorine in Medicinal Chemistry. *J. Med. Chem.* **2015**, *58*, 8315−8359.
(86) Zhou, Y.; Wang, J.; Gu, Z.; Wang, S.; Zhu, W.; Aceña, J. L.; Soloshonok, V. A.; Izawa, K.; Liu, H. Next Generation of Fluorine-Containing Pharmaceuticals, Compounds Currently in Phase II−III Clinical Trials of Major Pharmaceutical Companies: New Structural Trends and Therapeutic Areas. *Chem. Rev.* **2016**, *116*, 422−518.
(87) Johnson, E. R.; Keinan, S.; Mori-Sánchez, P.; Contreras-García, J.; Cohen, A. J.; Yang, W. Revealing Noncovalent Interactions. *J. Am. Chem. Soc.* **2010**, *132*, 6498−6506.
(88) Johansson, M. P.; Swart, M. Intramolecular Halogen−Halogen Bonds? *Phys. Chem. Chem. Phys.* **2013**, *15*, 11543−11553.
(89) Wang, W.; Foley, K.; Shan, X.; Wang, S.; Eaton, S.; Nagaraj, V. J.; Wiktor, P.; Patel, U.; Tao, N. Single Cells and Intracellular Processes Studied by a Plasmonic-Based Electrochemical Impedance Microscopy. *Nat. Chem.* **2011**, *3*, 249−255.
(90) Sasmal, D. K.; Ghosh, S.; Das, A. K.; Bhattacharyya, K. Solvation Dynamics of Biological Water in a Single Live Cell under a Confocal Microscope. *Langmuir* **2013**, *29*, 2289−2298.
(91) Johansson, M. P.; Swart, M. Subtle Effects Control the Polymerisation Mechanism in α-Diimine Iron Catalysts. *Dalton Trans.* **2011**, *40*, 8419−8428.
(92) Pantsar, T.; Poso, A. Binding Affinity via Docking: Fact and Fiction. *Molecules* **2018**, *23*, No. 1899.

DOI: 10.1021/acs.molpharmaceut.9b00437
Mol. Pharmaceutics 2019, 16, 3600−3608